applied sciences

MDPI

Article

Assessment of Fatigue Lifetime and Characterization of Fatigue Crack Behavior of Aluminium Scroll Compressor Using C-Specimen

Sang-Youn Park [1], Jungsub Lee [1], Jong-Tae Heo [2], Gyeong Beom Lee [2], Hyun Hui Kim [2] and Byoung-Ho Choi [1,*]

[1] School of Mechanical Engineering, Korea University, Seoul 02841, Korea; magicparkkor@korea.ac.kr (S.-Y.P.); bouce@korea.ac.kr (J.L.)
[2] R&D Center, LG Electronic Inc., Seoul 08503, Korea; Hjt.heo@lge.com (J.-T.H.); gyeongbeom.lee@lge.com (G.B.L.); hyunhui.kim@lge.com (H.H.K.)
* Correspondence: bhchoi@korea.ac.kr; Tel.: +82-2-3290-3378

Received: 31 March 2020; Accepted: 2 May 2020; Published: 6 May 2020

Abstract: Currently, a scroll compressor is used in many industrial fields; hence, research on its reliability is important. The major loading type during operation is pressure. However, unexpected contact between scroll compressors typically occurs, and thus, the severe loading condition should be considered. To consider this condition, the study modified the scroll compressor's structure to a C-type specimen. The study applied cyclic axial load in the specimen. The main objective of the study is to define a proper fatigue life method for the aluminium scroll compressor and proper finite element method (FEM) modeling. To define the method, the study included a case study for various parameters, such as mean stress effects. Furthermore, a crack propagation study is presented. In the study, the Darveaux method that considers the Bauschinger effect of ductile material is used. It is expected that the consideration of the parameters can help define the fatigue life assessment of an aluminium scroll compressor.

Keywords: life assessment; crack initiation; crack propagation; finite element method; scroll compressor

1. Introduction

In recent years, scroll compressors have been widely used in the automobile industry. They are operated under axial and radial loading conditions [1]. The rotation of the scroll leads to pressure and temperature changes. Thus, reliability is an important issue for the scroll. Yaubin Yang [2] attempted to simulate the pressure using ANSYS software. This research studied thermal stress during operation. Furthermore, Christophe Ancel [3] examined fatigue simulation via nCode DesignLife. Christophe used Dang Van analysis to assume the pressure during the operation. The dynamic model was studied by Qiang et al. [4]. He defined the scroll compressor's dynamic motion using dynamic characteristics such as pressure distribution, tangential force, and axial force. Furthermore, the accelerated condition was studied by Chang [5]. This study carried out research about wear under the accelerated condition. By using temperature as a parameter, we can define the crack initiation condition more thoroughly. Various types of gas force in scroll compressors were considered by Wang et al. [6]. By calculating the axial and radical force of gas during cycle, they ran the ANSYS program to calculate the deformation of the scroll. Dominique Gross [7] studied rotation speed. In Gross's study, the structure received axial, tangential and friction forces. For various RPM, they calculated force, which is sometimes more serious for the structure than pressure. After these processes, they predicted fatigue life with the stress–life curve of the material. To reduce the contact force, Lantian Ji [8] applied diamond-like carbon (DLC) film to the compressor. By reducing friction force, resistance can be reinforced. The commonality of the studies [2–7] is that they only calculated regular operation, and did not consider the scroll compressor itself. However, during the operation, the scroll compressor came under an unexpected loading condition, specifically, contact with the counterpart, i.e., the fixed scroll. Although previous research mentioned that the scroll compressor easily succumbs to failure during the operation, there is only a small amount of research which concentrates on the scroll compressor itself. Even though they ran the finite element method (FEM) for the scroll compressor, the validation of the structure was operated under the operating condition, which was dominated by pressure and thermal conditions in those references. Thus, the design of more conservative experiments is needed, which was not studied in previous research. To achieve this requirement, the study modified the scroll compressor to a C-specimen, thereby making it possible to apply concentrated force at the weak point. Furthermore, the fatigue parameter should also be considered with changes in the loading condition. This is because previous research [2,3,5,7] tends to focus on high cycle fatigue under elastic deformation. To recommend a proper fatigue parameter, fatigue life should be divided into two regions: initiation and propagation [9].

Crack initiation follows Miner's rule [10]. The rule states that, although the application of stress may not be sufficient to induce failure, the accumulation of repeating stress can lead to failure. If the damage accumulation arrives at one, then it implies crack initiation. The Stress–life (S-N) curve method is generally applied [9] to determine this cycle. This method is advantageous because measurements can be easily performed. The relationship between amplitude stress and fatigue cycle is given in Equation (1) as follows; [9].

$$\sigma_a = \sigma'_f \times (2N)^b \tag{1}$$

where N is the life cycle, σ_a is amplitude stress, σ'_f is the fatigue strength coefficient and b is fatigue strength exponent.

In addition to the fatigue curve, the mean stress effects must also be considered. The mean stress effect is a counting method for correcting non-uniform loading conditions [9]. Typically, the Goodman method (Equation (2)) and Gerber method (Equation (3)) [9] are used to correct non-uniform loading conditions. The Gerber method is less conservative when compared with the Goodman method. Additionally, in case of brittle materials, both methods tend to be similar to the Goodman method [9]. However, actual test data tend to exist between the Goodman and Gerber lines.

$$\frac{\sigma_a}{\sigma_{ar}} + \frac{\sigma_m}{\sigma_u} = 1 \tag{2}$$

$$\frac{\sigma_a}{\sigma_{ar}} + \left(\frac{\sigma_m}{\sigma_u}\right)^2 = 1 \tag{3}$$

where σ_{ar} is the equivalent fully reversed stress amplitude resulting in the same fatigue life, σ_a is the amplitude stress, σ_m is the mean stress and σ_u is the ultimate stress.

However, the methods tend to be inaccurate in severe loading conditions wherein plastic deformation can occur in the structure. The strain–life (ε-N) curve should be considered to solve the problem [11]. The method is advantageous because it can depict the Bauschinger effect of a material. By highlighting the Bauschinger effect, the method can consider the plastic deformation of the material between loading and unloading regions. The method is given in Equation (4) as follows; [11].

$$\frac{\varepsilon_a}{2} = \frac{\sigma'_f}{E} \times (2N)^b + \varepsilon'_f (2N)^c \tag{4}$$

where ε_a is the strain amplitude, σ'_f is the fatigue strength coefficient, N is life cycle, E is young's Modulus, b is the fatigue strength exponent, ε'_f is the fatigue ductility coefficient and c is the fatigue ductility exponent.

With respect to the strain(ε)–life(N) curve, there are two mean stress effect correction models, the Morrow (Equation (5)) [12] and Smith Watson Topper (SWT) (Equation (6)) models [13]. Ince et al. [14] indicated that the SWT model can apply changes in the load by calculating the energy that is multiplied with σ_{max}. This method is rather flexible, especially in high loading conditions.

$$\frac{\varepsilon_a}{2} = \frac{\sigma'_f - \sigma_m}{E}(2N)^b + \varepsilon'_f\left(\frac{\sigma'_f - \sigma_m}{\sigma'_f}\right)^{\frac{c}{b}}(2N)^c \tag{5}$$

$$\sigma_{max}\varepsilon_a = \frac{\left(\sigma'_f\right)^2}{E}(2N)^b + \varepsilon'_f\sigma'_f(2N)^{b+c} \tag{6}$$

where σ_{max} is the max stress during the cycle.

Based on these mean stress effects, many researchers developed models. Ince [15] suggested a multiaxial fatigue damage model based on strain energy. By considering strain shear energy, multi axial fatigue life can be considered. This method can also be adopted in distortion [16]. The form of energy was similar with that of SWT, which can be calculated by multiplying the strain and force of each type. There is little research applying Optistruct in the scroll compressor. However, there are another cases using Optistruct in fatigue simulation. Kim [17] calculated the fatigue life of the skate frame using FEM. In this study, he studied the surface effect and size effect, which can modify the fatigue limit. Musaddiq [18] compared the stress–life and strain–life curve in calculating the fatigue life of the joint prosthesis using FEM. He suggested that, for composite structures which receive excessive force, the strain–life curve is a proper parameter rather than the stress–life curve.

The fatigue lifetime of a structure can be divided into three mechanisms, i.e., crack initiation, crack propagation and dynamic instability. Among them, the time for dynamic instability is extremely short compared with the other two mechanisms. However, the contribution of crack propagation on the entire lifetime of a structure should be considered, unless the material fabricating a structure is brittle enough. Therefore, the lifetime of the scroll compressor should be studied by considering both the crack initiation and crack propagation behaviors. Hence, crack propagation should be considered to predict the lifetime until failure of the scroll compressor. The general method to depict crack propagation is the Paris law as follows; [19,20].

$$\frac{\mathrm{da}}{dN} = \Delta G > G_{1c} \tag{7}$$

where N is the life cycle, a is the length of the crack, G is the energy release rate, G_{1c} is the critical energy release rate.

This equation presents that if the energy release rate exceeds critical energy release rate, the crack propagates. This method is based on the linear elastic fracture mechanism (LFEM). Thus, if plastic deformation occurs in the structure, it tends to be inaccurate. To compensate for the weakness, the Darveaux method [20,21] should be considered (Equation (8) and Figure 1). By using strain energy density per cycle, the Darveaux coefficient is calculated as follows; [20,21].

$$N_0 = c_1(\Delta w)^{c_2},\ D_{N+\Delta N} = D_N + \frac{\Delta N}{L}c_3(\Delta w)^{c_4}\ (c_1, c_2, c_3, c_4 - material\ constant) \tag{8}$$

where N_0 is cycle number for damage initiation, Δw is inelastic hysteresis strain criteria. D_N is damage variable for degradation stiffness assumption. Thus, the degradation of the element can be calculated as follows; [20].

$$\sigma = (1 - D)\overline{\sigma},\ \text{is the stress of the current increment.} \tag{9}$$

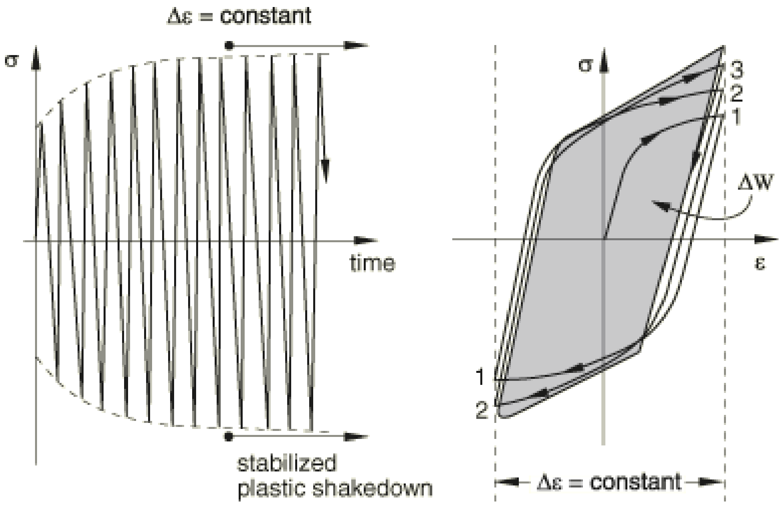

Figure 1. Plastic shakedown in a direct cyclic analysis [20].

The Darveuax method was used in many recent studies. Liulu [22] used the Darveux method to predict solder joints. By tracking individual solder failures, he mentioned that the Darveuax method can depict the change of inelastic region during repeated cyclic load. Thus, he suggested that the Darveuax method have advantages for depicting ductile material due to the inelastic strain energy density accumulated per cycle. Liuyang [23] proposed a method to calibrate the damage material parameters using both the Darveuax method and the strain–life curve. Even though there was no recent research which applied the Darveuax method to the scroll compressor, these recent studies have become helpful examples.

In the study, a parametric investigation is presented to determine the appropriate parameter for the customized C-specimen test. The entire cycle is calculated separately by dividing the initiation and propagation cycles. The crack initiation cycle is calculated by using Altair Optistruct software, which can accumulate element damage during cyclic loading. Specifically, ABAQUS 6.14 is used to calculate the crack propagation cycle. The specific results of the analysis are expected to aid in determining safe specifications of the scroll compressor.

2. Experiments

The scroll compressor used in this study is made of a silicon-manganese aluminium alloy, i.e., Al 4007A, as it is quite difficult to evaluate fatigue characteristics in the scroll compressor due to its complicated geometry and loading conditions. Therefore, a newly designed specimen, by considering the most dangerous region under operating conditions, is proposed and used in this study. To design the customized C-specimen, the stress distribution and deformation profile during the operation are considered, as shown in Figure 2. Prior to performing the experiment with the C-specimen, 4007A's material fatigue curve (S-N curve) was evaluated. A rotary bending test machine from Shimadzu Corporation, Kyoto, Japan was utilized. The advantage of the machine is that it increases speed to 50 Hz, which is five times faster than a tensile test machine. Furthermore, the rotary bending machine's fatigue R-ratio corresponds to −1, which is the ideal number for the fatigue curve.

As previously mentioned, the structure of C-specimen was revised based on the operating conditions, as shown in Figure 2, to apply severe loads comparable with the pressure. By removing a part of the wrap, the experimental device can accurately apply a vertical load at Point A, which is the weak point during scroll compressor operation as per operation and simulation data. The experimental device for the fatigue test of C-specimen was MTS 810 (MTS Systems Corp., Minneapolis, MN, USA). An additional guide structure was designed and used to prevent unexpected loading types (e.g., tangential loading between zig and wrap) as shown in Figure 3. The operation frequency was 10 Hz, and the R-ratio of the loading condition was 0.05. Additionally, five amplitude loads were applied as follows: 1900, 1662.5, 1444, 1140, and 948 N.

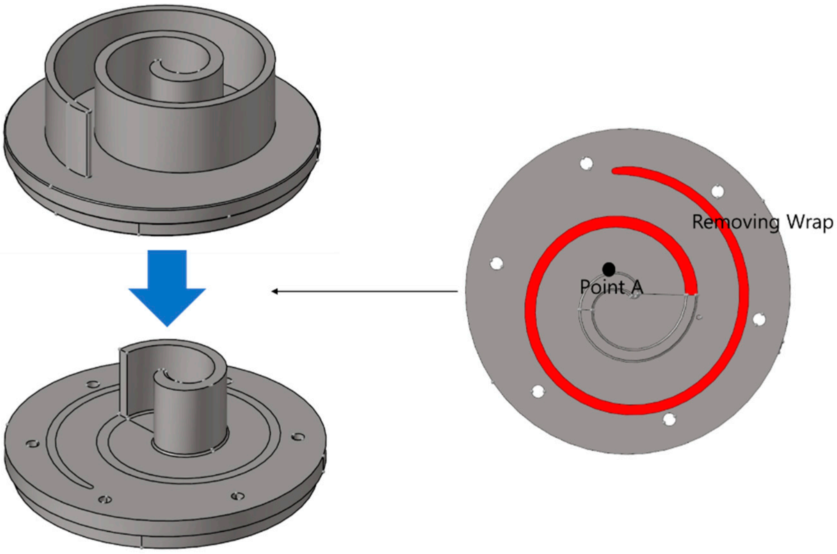

Figure 2. Modified scroll compressor to C-specimen.

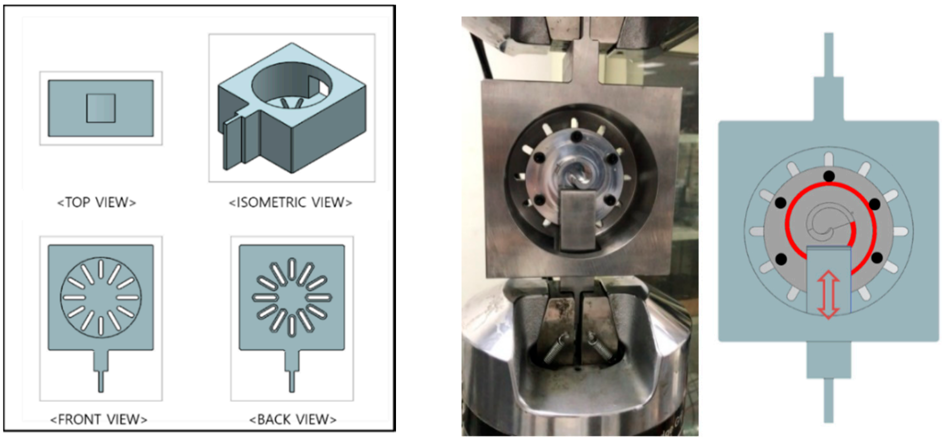

Figure 3. Guide structure (left) and experiment setting (right).

3. Finite Element Modeling Information

3.1. Material Information

Aluminium 4007A was used as the material for the scroll compressor [24]. The composition of the material is described in Table 1. The 4000 series aluminium contains more than 1% silicon, and thus the material is generally characterized with high yield strength and low elongation when compared with that of other aluminium materials.

Table 1. Composition of the aluminium alloy 4007A [24] (unit: %).

Elements	**Al**	**Si**	**Mn**	**Fe**	**Ni**	**Cr**
Percentage	96.3	1.4	1.2	0.7	0.3	0.1

The mechanical properties of the tensile test, listed in Table 2, were used in Optistruct and ABAQUS. In order to use Optistruct, stress–life and strain–life curves should be used. The parameters used in Optistruct are listed in Table 3. Essentially, fatigue strength coefficient (σ'_f) and exponent (b) are identical in the S-N and ε-N curves. They can be calculated from the S-N curve (Figure 4) measured from the rotary bending machine. The equation used for the other parameters is calculated from [9].

Table 2. Mechanical properties of Al 4007A.

Elements	Young's Modulus	Yield Strength	Tensile Strength	Elongation to Break
Percentage	70.0 GPa	340 Mpa	405 Mpa	0.09

Table 3. Strain–life curve information in Optistruct.

Symbol	$\sigma_f^{'}$	$\varepsilon_f^{'}$	b	C	$K^{'}$	$n^{'}$
Value	723 Mpa	0.11	−0.091	−0.705	455 Mpa	0.12
Equation	-	Elongation	-	$n' = \frac{c}{b}$ [9]	From S-S curve [9]	From S-S curve [9]

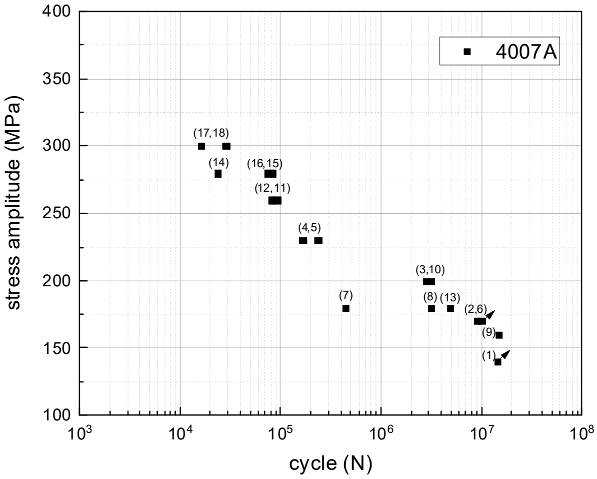

Figure 4. Stress–Life curve of Al 4007A.

With respect to the Paris law and Darveaux method, the following parameters in Table 4 are used. If the model only considers Paris law, G_{1c} is used. To consider the Darveaux method, $c_1 \sim c_4$ should be added. The parameters were calculated from the cyclic S-S curve of the material from the tensile test machine.

Table 4. Values used in the Paris law and Darveux coefficient in ABAQUS extend finite element method (XFEM).

Symbol	G_{1c}	c_1(Cycles/MPa^{c_2})	c_2	c_3	c_4
Value	0.014 Mpa	0.9×10^{-7}	−0.1	6×10^{-5}	0.327

3.2. FEM Modeling

3.2.1. Loading and Boundary Condition

Geometry and boundary conditions are identical for simulations in Optistruct and ABAQUS. The size of the element was 0.5 mm in Optistruct and ABAQUS. The type of the element was a hexagon. The force acting on the nodes was used to depict the loading condition. The total amount of loads was summary of the load given at each node. The red area shown in Figure 5 is the fixed area in FEM. This is because if the guide structure is used, the complete back side of C-specimen would be fixed firmly, even though only six bolting points were used in the actual experiment. This is the same effect as the structure fixed on the wall. Thus, all degree of freedom (DOF) of nodes on the back side were fixed. In the study, crack initiation and crack propagation were measured separately. Total cycle can be counted via a summary of cycle results of Optistruct and ABAQUS XFEM.

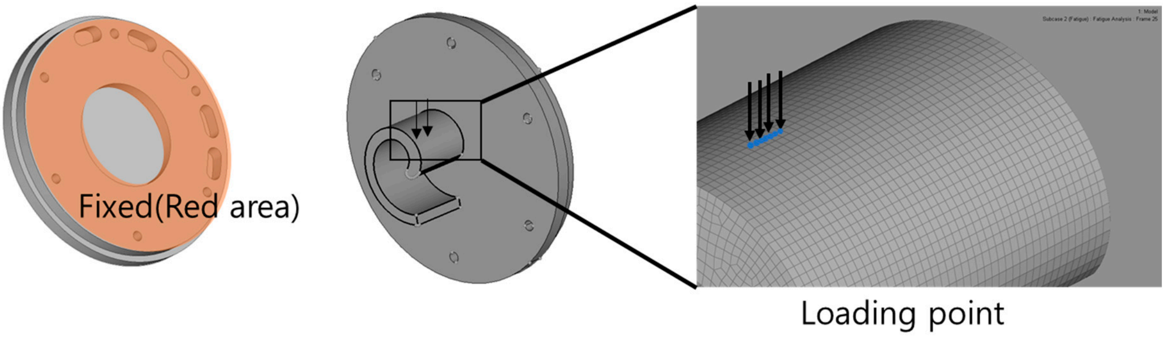

Figure 5. Boundary and loading conditions of the finite element method (FEM).

3.2.2. Crack Initiation

With respect to crack initiation, the study used Altair Optistruct 2018. If the crack occurred, it represented the damage contour as 1 (Figure 6) based on the Miner's rule [10]. Both Optistruct and ABAQUS software run fatigue based on one static step. This means that one cycle step should be utilized as an initial condition before using the fatigue step to run the fatigue module. The study used both stress–life curve and strain–life curve in Optistruct. Thus, by performing the parametric study for various mean stress effects such as the Goodman, the Gerber, the Morrow and the SWT, the study recommends proper parameters by comparing the results of the experiment and FEM.

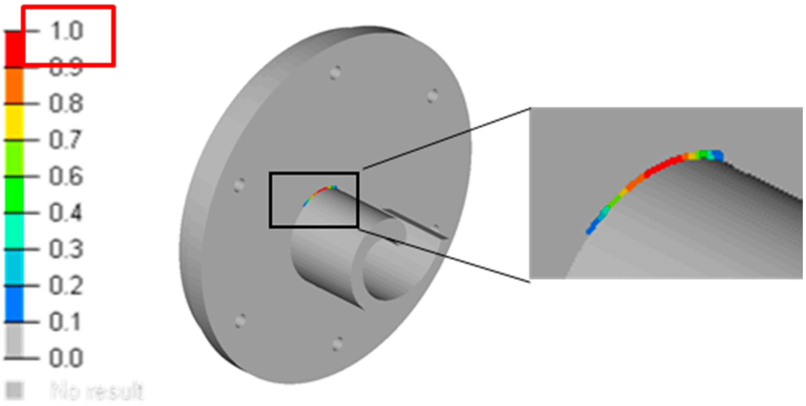

Figure 6. Damage contour of fatigue simulation in Optistruct.

3.2.3. Crack Propagation

Crack propagation was examined via ABAQUS extend finite element method (XFEM). When ABAQUS XFEM is used, it is assumed that crack is already initiated, and that the location of crack initiation is accurate. Specifically, ABAQUS XFEM depicts the crack propagation line that connects between virtual nodes, which are not on the element. The advantage of the method is that it conserves the stiffness of the structure because it does not delete the element. The basic enrichment function of the XFEM is in Figure 7 and Equations (10)–(12) [25].

$$u = \sum_{I=1}^{N} N_I(x)\left[u_I + H(x)a_I + \sum_{\alpha=1}^{4} F_\alpha(x)b_I^\alpha\right] \tag{10}$$

$$H(x)\begin{cases} 1, & if\ (x-x^{*})*n \geq 0 \\ -1\,, & otherwise \end{cases} \quad x^{*} \text{ is the point on the crack closet to x} \tag{11}$$

$$F_{\alpha}(x) = \left[\sqrt{r}sin\frac{\theta}{2},\ \sqrt{r}cos\frac{\theta}{2},\ \sqrt{r}sin\theta sin\frac{\theta}{2}, sin\theta cos\frac{\theta}{2}\right], \tag{12}$$

where $N_1(x)$ is the usual nodal shape functions and u_I is the displacement vector of the elements in the part. $H(x)$ is the discontinuous function which can be presented like equation 11 [25]. $F_{\alpha}(x)$ is the stress asymptotic function of crack tip can be represented as Equation (12) [25]. (r, θ) in Equation (12), is polar coordinate from origin crack tip. a_I and b_I^{α} in Equation (10), are nodal enriched degrees of freedom vectors of $H(x)$ and $F_{\alpha}(x)$.

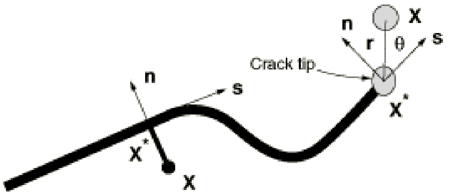

Figure 7. Illustration of normal and tangential coordinates for a smooth crack [25].

Equation (10) consists of the near tip asymptotic functions that capture singularity around the crack tip and a discontinuity that represents the jump in displacement across the crack surfaces. u_I is applicable for all nodes. $H(x)a_I$ is cut by crack. $\sum_{\alpha=1}^{4} F_{\alpha}(x)b_I^{\alpha}$ is used only for nodes whose shape function is cut by the crack tip.

To decide the direction parameter, (r, θ), the XFEM crack looks for the location which satisfies damage initiation criterion. Without this criterion, the crack will just extend without a crack path change ($\theta = 0$). If the Paris law is used without the Darveuax coefficient, the onset of delamination will follow Equation (7), which satisfies $\Delta G > G_{1c}$. However, if the damage initiation criterion is used, such as the Darveuax method, it will change the damage variable of the element, D, used in Equation (8). This means that ΔG changes due to degradation of the element. This degradation can change the crack path by changing stress distribution near the crack tip based on Equation (9).

To count the cycle, the direct cycling step in ABAQUS was used. Based on the results of the static step, the program calculates the cycle to propagate. The important assumption made in order to run ABAQUS XFEM is that the location of the initial crack is exact. In the study, the crack initiation point is same with the location of Optistruct results. Thus, the crack initiation point is based on the results of Optistruct as presented in Figure 6. Constants for the empirical Paris law are considered in XFEM. To apply the Darveux coefficient, a material keyword, * Damage initiation/evolution, should be used. A basic elastic–plastic curve and boundary condition are identical to those of Optistruct. The effect of the Darveuax method is presented in the next chapter, by comparing the model which used the Darveuax method in its material keyword and the model that did not. If the Darveux method is not used, the crack will be only be propagated with the fracture criterion keyword using the critical energy release rate without strain energy change.

4. Results

4.1. Experiment

Figure 8 shows an example of the load–displacement curve of the C-specimen. The displacement tends to rise significantly when the crack initiates and propagates. This is because after the crack initiates, the wrap tends to bend more than before.

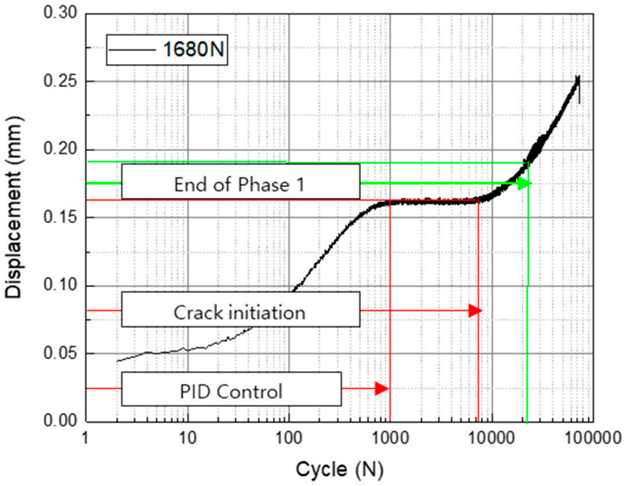

Figure 8. Example of displacement–cycle curve for the c-specimen at 1680 N.

The typical shape of the crack is shown in Figure 9. The crack initiated at the root below the loading point (Figure 9). After a crack initiates, the crack propagates along the wrap's root shape (Phase 1 in Figures 8 and 9). After a certain number of cycles from the end of Phase 1, the crack changes direction outside from the wrap root (Phase 2 in Figure 10). In this phase, the displacement is approximately about 1.2 times larger than the displacement of crack initiation. The fracture mode implies fracture of the wrap. The length of Phase 1 tends to increase when the applied load decreases. This is because a decrease in the load delays severe fracture and Phase 2 in the wrap.

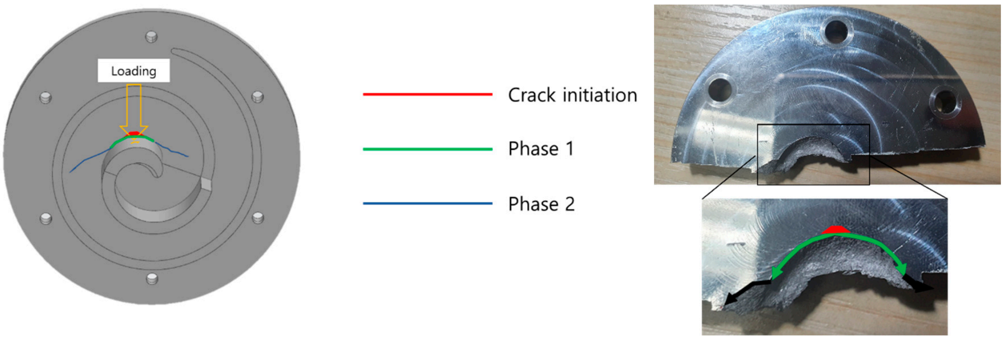

Figure 9. Crack shape picture and example of crack occurrence when the amplitude load is 1920 N.

Figure 10 shows the load amplitude and cycle curve of crack initiation, namely Phase 1. The curve shape of the crack initiation and Phase 1 is similar. Hence, it is estimated that all phases are affected by the same mechanical behavior. For example, in the case of the load exceeding 1900 N, at which plastic deformation occurs, all phases in progress should consider the Bauschinger effect.

4.2. Finite Element Method

4.2.1. Crack Initiation

In this study, a parametric investigation with respect to two parameters is performed. The first parameter is criterion of damage. We recommend using max principal stress as a criterion. This is because if the von Mises criterion is applied, then the damage contour represents the crack initiation point at the maximum compression location as opposed to the tensile maximum point (Figure 11). However, in the experiment, no crack is observed at this location. If the max principal stress is selected as the criterion, it identifies the accurate location, which is similar to the results of the experiment.

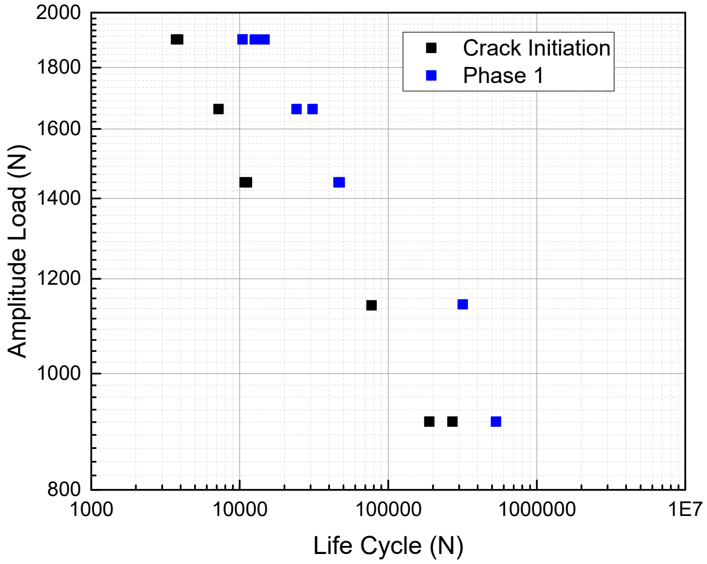

Figure 10. Load amplitude–Cycle curve of the C-specimen.

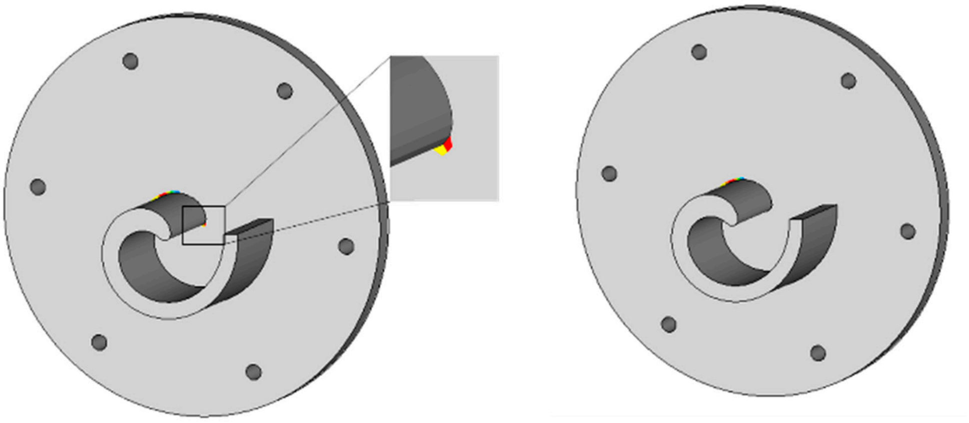

Figure 11. Damage contour of fatigue FEM for various criteria: von Mises (left)/max principal stress (right).

With respect to stress–life curve, the Gerber and Goodman methods were examined. Figure 12 shows the FEM results of the fatigue analysis when the Goodman and Gerber methods were used. As mentioned in the previous chapter, the Goodman method is a conservative method that exhibits a lower cycle than the Gerber method. Thus, when the applied amplitude load exceeds 1500 N, the results of the Goodman method are relatively inaccurate when compared with that of the Gerber method. If the applied load is sufficiently low, then the experimental results are between those of the Goodman and Gerber methods.

With respect to strain–life curve, the Morrow and SWT models were compared. Figure 13 shows the amplitude of the load and life cycle curve of the structure. Under a load of 1500 N, there is no significant difference between the Morrow and SWT. However, increases in the load increases the difference between the two. This implies that SWT can correct high loading effects by calculating the energy of the structure. It is expected that the SWT can model the experiment more accurately than the Morrow as the load in the experiment increases. The result is similar to that obtained in a study by Dowling [26], which indicates that SWT is more suitable for the aluminium alloy as opposed to the Morrow.

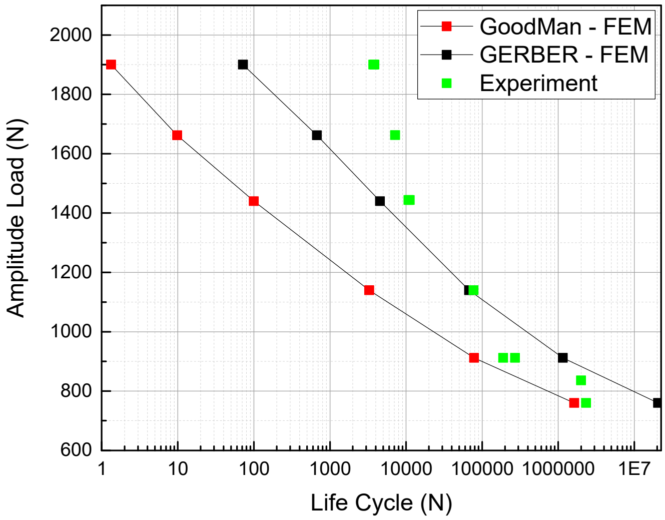

Figure 12. Comparison of the FEM and experiment when the stress–life (S-N) curve is applied in FEM.

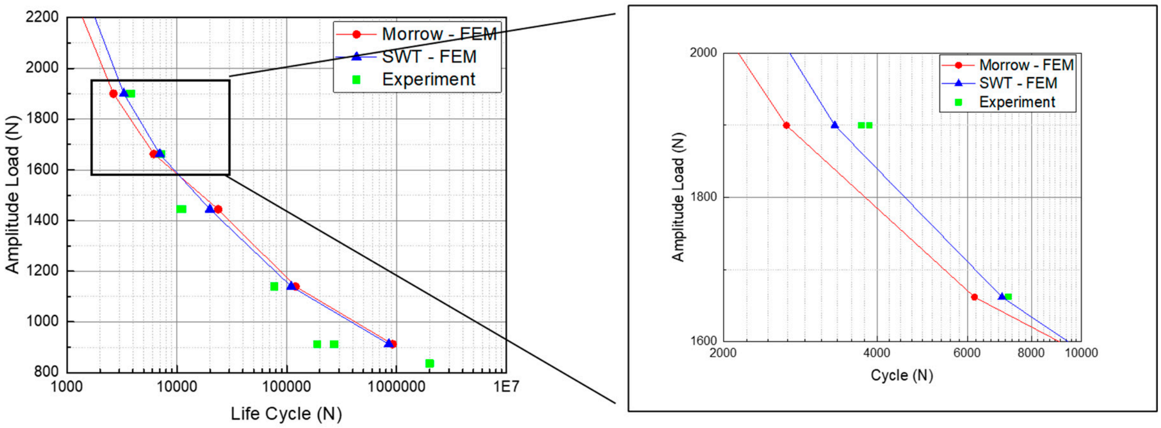

Figure 13. Comparison between FEM and experiment when ε-N curve is applied in FEM.

4.2.2. Crack Propagation

In this subsection, crack propagation models that use the Paris law and hysteresis energy method are compared and validated. Figure 14 shows the crack propagation characteristics predicted by the ABAQUS XFEM when the applied load is varied. It is observed that, in the loading condition under a load amplitude of 1400 N, the difference as to whether the Darveaux method is used is not significant (e.g., Figure 14a with the load amplitude of 916N). This is because plastic deformation does not dominate the structure in the loading condition due to the low loading amplitude. However, if the load amplitude exceeds 1900 N, then the difference is based on the usage of the Darveaux method. As shown in Figure 14b, the direction of the crack is slightly upward when the Darveaux method is not used. This is because the structure cannot apply the Bauschinger effect during crack propagation if the Darveaux method cannot be applied in the structure, and thus the stiffness of the structure is weak when compared with the model with the application of Darveaux method. This assumption can also be proven by the displacement–cycle curve as shown in Figure 15. In the absence of the Darveaux method, the FEM analysis does not reflect the Bauschinger effect. Thus, the speed of crack propagation exceeds that of the experiment and FEM model, which adds the Darveaux coefficient.

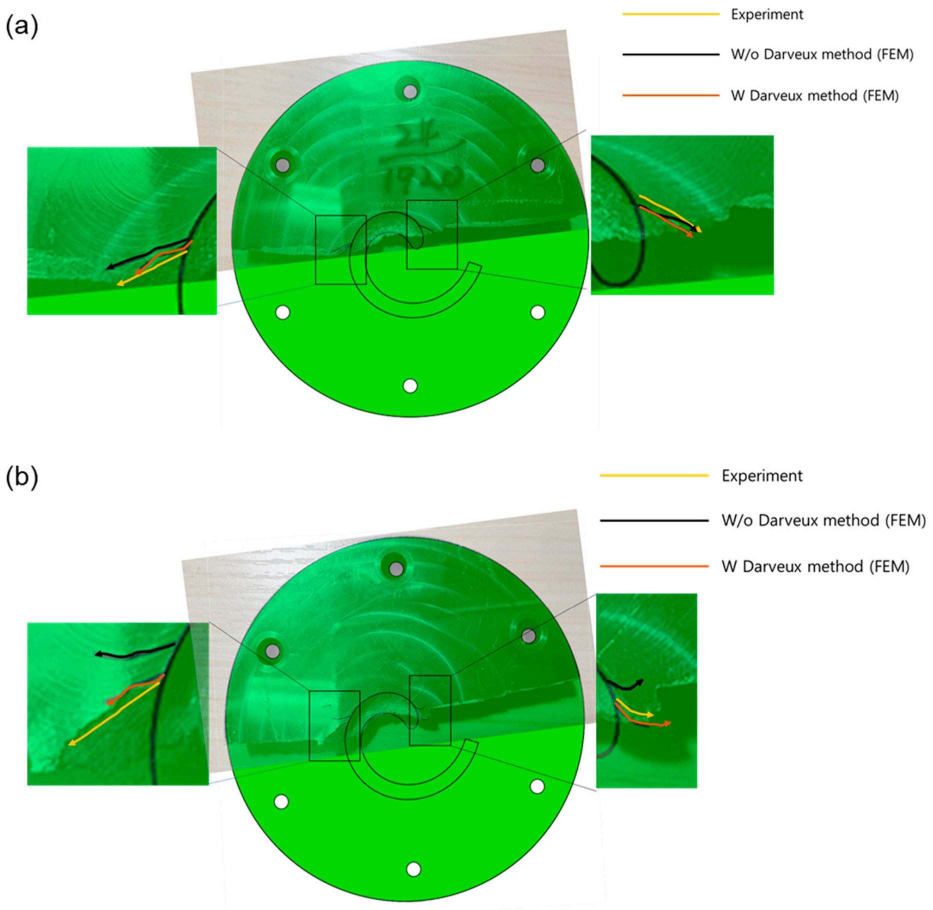
(a)
Experiment
W/o Darveux method (FEM)
W Darveux method (FEM)
(b)
Experiment
W/o Darveux method (FEM)
W Darveux method (FEM)

Figure 14. Comparison of the crack path between experiment and FEM. (**a**) Amplitude load of 916N. (**b**) Amplitude load of 1920N.

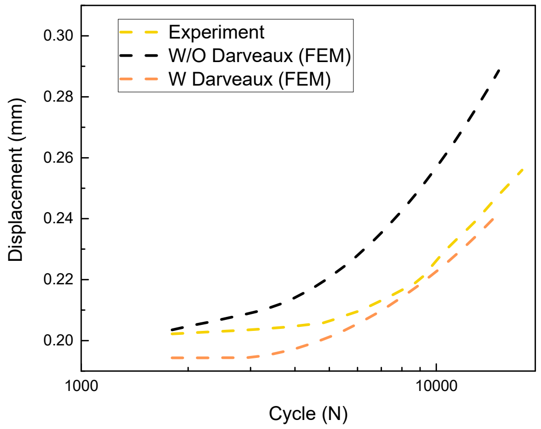

Figure 15. Displacement comparison between FEM and experiment from crack initiation to end of Phase 1 (before this cycle, it is assumed that cycle before crack initiation is correct).

5. Conclusions

In the study, a conservative method for scroll compressor designs was used. The study revised the structure of the scroll compressor by removing part of the wrap. This modification makes zig contact possible on the weak point directly. The life cycle of the scroll compressor was measured continuously after crack initiation. The change of the crack path can be estimated in the displacement-cycle curve of the experiment from the change of the slope. The study divides this region as Phase 1, where the crack changes direction outside from the wrap root. Additionally, various parameters were examined via the FEM. A parametric study was included to determine the correct parameters, such as mean stress effects and crack propagation model.

With respect to the crack initiation cycle, the mean stress effect was examined. For the S-N curve, the Goodman and Gerber method were compared. In a relatively high loading condition, the Gerber method records more cycles than the Goodman method. With a decrease in the loading condition, the experimental results were between the results of the Goodman and Gerber methods. Thus, the Gerber method is recommended while using the S-N curve for the C-specimen fabricated from 4007A. With respect to the ε-N curve model, the Morrow and SWT were compared. In the high loading condition over 1900 N, the SWT tends to be more accurate than Morrow. The energy calculation indicates that the SWT can more efficiently depict the high loading cycle of an aluminium structure.

With respect to crack propagation, the effect of the Darveaux method was examined. In a relatively low loading cycle, there is no significant difference as to whether or not the Darveaux method is used. This is because plastic deformation does not dominate during the fatigue cycle in the conditions. However, in the loading condition over 1900 N, the results differed based on the usage of the Draveaux method. Given its plastic deformation, the model that did not use the Draveaux method tended to crack and propagate upward. The model that used the Draveaux method tended to be more similar than the other model.

In the study, the behavior of the C-specimen is evidently dominated by the Bauschinger effect. To depict the fatigue result, the use of SWT and the Draveaux method are recommended. Thus, it is expected that conservative design can be obtained by using the results of the study.

Author Contributions: Project administration, B.-H.C.; Software, S.-Y.P.; Supervision, J.-T.H.; Validation, J.L., G.B.L. and H.H.K.; Writing–original draft, S.-Y.P. All authors have read and agreed to the published version of the manuscript.

Funding: The research was funded by LG Electronics corporations Inc.

Acknowledgments: The author would like to acknowledge the sharing the scroll compressor and the specimen of LG Electronics Inc.

Conflicts of Interest: The authors declare no conflict of interest.

Nomenclature

σ_a	Strength amplitude
σ_m	Mean stress
σ_u	Ultimate tensile strength
N	Loading cycle
ε_a	Strain Amplitude
σ'_f	Fatigue strength coefficient
b	Fatigue strength exponent
c	Fatigue ductility exponent
ε'_f	Fatigue ductility coefficient
K'	Cyclic strength coefficient
n'	Cyclic strain hardening exponent
D	Damage variable of the element
E	Modulus of elasticity
G	Energy release rate
w	Strain energy density
L	Characteristic length with respect to integration point

References

1. Morishita, E.; Sugihara, M.; Inaba, T.; Nakamura, T. Scroll compressor analytical model. In Proceedings of the International Compressor Engineering Conference, West Lafayette, IN, USA, 11–13 July 1984.
2. Yang, Y.; Tang, Y.-J.; Chang, Y.-C. Static and dynamic analysis on R410A scroll compressor components. In Proceedings of the International Compressor Engineering Conference, West Lafayette, IN, USA, 12–15 July 2010.

3. Ancel, C.; Gross, D.; Guglielmi, L. Fatigue design for scroll compressor wraps. In Proceedings of the International Compressor Engineering Conference, West Lafayette, IN, USA, 12–15 July 2010.
4. Qiang, J.; Peng, B.; Liu, Z. Dynamic model for the orbiting scroll based on the pressures in scroll chambers–Part I: Analytical modeling. *Int. J. Refrig.* **2013**, *36*, 1830–1849. [CrossRef]
5. Chang, M.S.; Park, J.W.; Choi, Y.M.; Park, T.K.; Choi, B.O.; Shin, C.J. Reliability evaluation of scroll compressor for system air conditioner. *J. Mech. Sci. Technol.* **2016**, *30*, 4459–4463. [CrossRef]
6. Wang, H.; Tian, J.; Du, Y.; Hou, X. Numerical simulation of CO_2 scroll compressor in transcritical compression cycle. *Heat Mass Transf.* **2018**, *54*, 1395–1403. [CrossRef]
7. Gross, D.; Genevois, D. Scroll Wrap Additional Stress In Variable Speed Application. In Proceedings of the International Compressor Engineering Conference, West Lafayette, IN, USA, 9–12 July 2018.
8. Ji, L.; He, Z.; Han, Y.; Chen, W.; Xing, Z. Investigation on the Performance Improvement of the Scroll Compressor by DLC Film. In Proceedings of the IOP Conference Series: Materials Science and Engineering, University of London, UK, 9–11 September 2019.
9. Aliabadi, M. *Fundamentals of Metal Fatigue Analysis*; Bannantine, J.A., Comer, J.J., Handrock, J.L., Eds.; Prentice Hall Publishers: Upper Saddle River, NJ, USA, 1990; pp. 2–27.
10. Miner, M. Cumulative fatigue damage. *J. Appl. Mech.* **1945**, *12*, A159–A164.
11. Aliabadi, M. *Fundamentals of Metal Fatigue Analysis*; Bannantine, J.A., Comer, J.J., Handrock, J.L., Eds.; Prentice Hall Publishers: Upper Saddle River, NJ, USA, 1990; pp. 40–72.
12. Morrow, J. Fatigue properties of metals. In *Fatigue Design Handbook*; Society of Automotive Engineers: Pittsburgh, PA, USA, 1968; pp. 21–30.
13. Smith, K. A stress-strain function for the fatigue of metals. *J. Mater.* **1970**, *5*, 767–778.
14. Ince, A.; Glinka, G. A modification of Morrow and Smith–Watson–Topper mean stress correction models. *Fatigue Fract. Eng. Mater. Struct.* **2011**, *34*, 854–867. [CrossRef]
15. Ince, A.; Glinka, G. A generalized fatigue damage parameter for multiaxial fatigue life prediction under proportional and non-proportional loadings. *Int. J. Fatigue* **2014**, *62*, 34–41. [CrossRef]
16. Ince, A. A mean stress correction model for tensile and compressive mean stress fatigue loadings. *Fatigue Fract. Eng. Mater. Struct.* **2017**, *40*, 939–948. [CrossRef]
17. Kim, H.K. Evaluation of Fatigue Endurance Foran Ultra Lightweight Inline Skate Frame. In *Advanced Materials Research*; Trans Tech Publications Ltd: Bäch, Switzerland, 2013.
18. Al-Ali, M.A.; Al-Ali, M.A.; Takezawa, A.; Kitamura, M. Topology Optimization and Fatigue Analysis of Temporomandibular Joint Prosthesis. *World J. Mech.* **2017**, *7*, 323–339. [CrossRef]
19. Paris, P.C. A rational analytic theory of fatigue. *Trend Eng.* **1961**, *13*, 9.
20. Abaqus. ABAQUS user's manual. In *Version 6.14 User's Guide*; Abaqus: Providence, RI, USA, 2014; p. Section 23.2.2.
21. Darveaux, R. Effect of simulation methodology on solder joint crack growth correlation and fatigue life prediction. *J. Electron. Packag.* **2002**, *124*, 147–154. [CrossRef]
22. Jiang, L.; Zhu, W.; He, H. Comparison of darveaux model and coffin-manson model for fatigue life prediction of bga solder joints. In Proceedings of the 2017 18th International Conference on Electronic Packaging Technology (ICEPT), Harbin, China, 16–19 August 2017.
23. Feng, L.; Qian, X. Low cycle fatigue test and enhanced lifetime estimation of high-strength steel S550 under different strain ratios. *Mar. Struct.* **2018**, *61*, 343–360. [CrossRef]
24. Association, A. *Aluminum Standards and Data*; Aluminum Association: Washington, DC, USA, 2013.
25. Abaqus. ABAQUS user's manual. In *Version 6.14 User's Guide*; Abaqus: Providence, RI, USA, 2014; p. Section 10.7.1.
26. Dowling, N.E. *Mean Stress Effects in Stress-Life and Strain-Life Fatigue*; SAE Technical Paper: Pittsburgh, PA, USA, 2004; p. 13.

© 2020 by the authors. Licensee MDPI, Basel, Switzerland. This article is an open access article distributed under the terms and conditions of the Creative Commons Attribution (CC BY) license (http://creativecommons.org/licenses/by/4.0/).